

Mössbauer study of the proximity gettering of cobalt atoms to He-induced nanosized voids in *c*-Si

W. Deweerd,* T. Barancira, S. Bukshpan,† S. Demuyneck, G. Langouche, K. Milants, R. Moons, J. Verheyden, and H. Pattyn

Katholieke Universiteit Leuven, Physics Department, Instituut voor Kern-en Stralingsfysica, Celestijnenlaan 200D, B-3001 Leuven, Belgium

(Received 27 November 1995; revised manuscript received 20 February 1996)

We observe a strong gettering of ion implanted ^{57}Co to the internal surface of empty nanosized voids in *c*-Si, hampering normal silicide formation. The cavities are introduced by implanting He far above the solubility limits and subsequent desorption at 700 °C during 30 min. After ^{57}Co implantation and thermal treatment, a previously unobserved Mössbauer spectrum was recorded that could be fitted consistently with two quadrupole doublets. They differ largely in binding strength and electric-field gradient V_{zz} and we preliminarily interpret them as an edge site (strong binding, smaller V_{zz}) and a surface site (loose binding, larger V_{zz}) at the internal surface of the faceted voids. The spectra are stable upon high-temperature annealing. [S0163-1829(96)07024-5]

I. INTRODUCTION

In recent years a huge amount of research has been dedicated to semiconductors concerning the severe requirements for the defect density and contamination concentration present during device processing. Especially the 3d-transition metals (Fe, Co, Cu, and Ni) and their silicide precipitates are known for their detrimental effects on Si-based devices, even at very dilute concentrations,¹ necessitating an efficient gettering. However, since thermal budgets reduce, not only is the getter efficiency important but also the possibility for a proximity gettering. “Distant” gettering techniques remove the impurities from the electrically active region by precipitation at the back side or in the bulk of the wafer.² In this context, the gettering effect of lattice disorder induced by ion implantation has been studied intensively. Recently Myers *et al.* found that the dangling bonds (DB’s) at the internal surface of empty nanosized voids in Si are very efficient for gettering transition metals.³ They prove that Cu can be dissolved from its silicide phase and subsequently trapped up to monolayer coverage of the internal surface of these voids. The corresponding binding energy is 2.2 ± 0.2 eV relative to Cu in solution, 0.5 eV higher than the solution enthalpy of the original silicide phase. Preliminary results on Ni indicate that a substantially smaller amount is trapped under similar conditions, tentatively ascribed to a less dense ordered structure of chemisorbed Ni on the surface. Other groups studied Au (Ref. 4), Fe (Ref. 5), or Pt (Ref. 6), each confirming the gettering effect of the voids. This paper reports on the feasibility of populating these voids with Co atoms. The first reason for this particular choice is that it forms the interesting CoSi_2 silicide.^{7,8} Controlled introduction of thin silicide layers becomes increasingly attractive for its applicability in device processing. Because of the high stability of CoSi_2 , with a solution enthalpy of 2.83 eV,⁹ it is not evident that trapping at the voids will occur. Secondly, in ^{57}Co we have an excellent mother isotope for Mössbauer spectroscopy, offering a way of probing the local atomic

environment by the hyperfine interaction with its nearest neighbors. Our primary concern is to microscopically “tag” these possibly numerous new getter sites.

II. SAMPLE PREPARATION

A. Cavity formation

The voids are produced by He implantation up to a local concentration of 6 to 8 at. % (Refs. 3,6,10,11), initially leading to bubble formation. By subsequent UHV annealing, almost all He desorbs from the bubbles, leaving behind larger but empty cavities. The average cavity diameter grows with increasing annealing temperature by migration and coalescence. At first the voids have a nearly spherical shape, although the most stable morphology is that of a truncated octahedron, achieved after longer annealing times.¹¹ No orientation, doping or type dependence has been observed. We used 380- μm -thick *n*-type (111)-oriented float zone Si with $\rho = 4000 \Omega \text{ cm}$. The He implantations were performed at the polished side with a fluence ranging between 6.7×10^{16} atoms/cm² at 16 keV and 1×10^{17} atoms/cm² at 30 keV followed by desorption at 700 °C during 30 min with a constant heating rate of 0.5 K/s. The desorption was monitored by attaching a He-sensitive detector to the pumping exit of the furnace. Within the experimental errors, all implanted He is accounted for. Transmission-electron microscopy (TEM) pictures (not depicted) confirm the presence of the voids with an average diameter of approximately 8–10 nm. For this case, Myers *et al.* report a total internal surface of the voids of 6–7 cm² per cm² of implanted Si surface,³ leading to approximately 3×10^{12} voids/cm². Similarly we can calculate the total number of DB’s at the internal surface, yielding 5×10^{15} DB’s/cm² or 1500 DB’s per void. The number of available DB’s will probably be significantly smaller due to local recombinations. After desorption, we performed a series of Rutherford backscattering spectrometry and channeling measurements (RBS-C) and compared the results with those for a sample in which only correlated damage due to Si

implantation is present (sample *d*, see Sec. II B). A detailed description of the experiments will be given elsewhere.¹²

B. He and ⁵⁷Co implantation

All samples were implanted at the Leuven Isotope Separator facility. Three of them contained cavities while one contained implantation-induced damage but no voids. Sample *a* was implanted with 1×10^{17} He/cm² at 30 keV, followed by desorption and a ⁵⁷Co implantation with a fluence of 1.65×10^{14} atoms/cm² at 80 keV at the opposite side of the He implantation. Sample *b* was implanted with 1×10^{17} He/cm² at 16 keV. Before desorption, ⁵⁷Co was implanted at 80 keV on the opposite side of the sample with a fluence of 1×10^{13} atoms/cm². Sample *c* was implanted with ⁵⁷Co at 90 keV with a fluence of 1.74×10^{14} atoms/cm². Afterwards He was introduced at the same side of the ⁵⁷Co implantation with an energy of 16 keV and a fluence of 6.7×10^{16} He/cm². Sample *d* was implanted with Si with a fluence of 5×10^{14} atoms/cm² at 60 keV and subsequently with 3×10^{14} atoms/cm² ⁵⁷Co and 7×10^{14} atoms/cm² ⁵⁹Co at 50 keV at the same side as the Si implantation. All implantations were performed at room temperature (RT) and under a certain angle to avoid channeling effects. For the ⁵⁷Co implantations, roughly half the flux consists of ⁵⁷Co atoms, the rest being ⁵⁷Fe atoms.

III. EXPERIMENTAL SETUP

A. Mössbauer experiments and analysis

Mössbauer experiments can be performed as an absorber or as a source measurement. For an absorber experiment at least 10^{16} ⁵⁷Fe atoms/cm² are needed. Source experiments, however, can be performed with as little as 10^{10} ⁵⁷Co atoms/cm².¹⁶ It should be mentioned that for source measurements the implanted parent isotope ⁵⁷Co determines the solubility and diffusion coefficient, and dominates the eventual binding site. It then decays to ⁵⁷Fe, which has a mean lifetime $\tau \sim 1 \times 10^{-7}$ s, much larger than the electronic relaxation time of most known systems so that no after-decay effects are expected and the observed electronic environment and binding strength are those of the daughter nucleus.¹⁵ This somewhat complex approach does not facilitate interpretation but it permits much lower implantation doses. All depicted Mössbauer experiments were performed at RT as constant acceleration source measurements in transmission geometry, using a SFC [Na₄Fe(CN)₆10H₂O] absorber with a thickness of 1 mg/cm² kept at RT. Least square fitting of the spectra was done assuming that all line shapes are Lorentzian, leaving the width of the lines as an adjustable parameter in order to minimize the number of components necessary to obtain a reasonable fit.^{17,18} In addition, temperature-dependent measurements of the recoil-free fraction *f* were done down to 4.2 K in order to extract the characteristic Mössbauer temperature Θ_M using the following formula:

$$f(T) = \exp \left\{ - \frac{6E_R}{k_B \theta_M} \left[\frac{1}{4} + \left(\frac{T}{\theta_M} \right)^2 \int_0^{\theta_M/T} \frac{x}{e^x - 1} dx \right] \right\}$$

with $E_R = \frac{E_0^2}{2Mc^2}$,

with $E_0 = 14.4$ keV and *M* the mass of a ⁵⁷Co atom. The procedure¹⁷ consists in fitting a series of spectra of the same sample measured at different temperatures in a consistent way. The linewidth *W* and the quadrupole splitting Δ are hereby taken to be the same for all spectra. The first iteration leaves δ free and puts the second-order Doppler (SOD) shift equal to 0. This gives a first approximation of *f*(*T*) that in turn gives an estimation of Θ_M . This then allows us to calculate SOD(*T*). In all subsequent iterations δ is taken to be consistent and the SOD is kept constant at the calculated value until the results converge within the experimental error.

B. ⁵⁷Co depth distribution

Another advantage of implanting radioactive probes is that they can be used as tracers for determining the depth distribution after thermal treatment. By measuring the relative intensity of the 14-keV γ peak at both sides of the sample, it is possible to extract the fraction of atoms at the ‘‘surface’’ (i.e., less than ~ 500 nm beneath the physical surface) at each side of the sample. We assume that there is no Co present in the bulk of the sample, justified by the vanishingly solubility at RT.⁹ The sides of the sample are labelled as *V* (void) and *N* (non) *V* (void). The surface fraction *c* of ⁵⁷Co atoms at the *V* side is determined by the following equation:

$$\frac{I_V(14 \text{ keV})}{I_{NV}(14 \text{ keV})} = \frac{c + (1-c)e^{-\mu d}}{ce^{-\mu d} + (1-c)},$$

where *d* is the thickness of the wafer and μ is the linear absorption coefficient. This nondestructive technique gives a first approximation of the changes in the distribution and has already been employed by Bergholtz¹⁹ in a slightly different way. The resolution, however, is insufficient to measure the amount of atoms that resides at the cavities. To do so we chemically etched the samples by anodic oxidation. This destructive technique consists of galvanostatic oxidizing the top atomic layers of the sample by an electrochemical reaction: $\text{Si} + 2\text{H}_2\text{O} \rightarrow \text{SiO}_2 + 4\text{H}^+ + 4e^-$. Since this reaction involves H₂O, a glycolethylene electrolyte is used instead of an aqueous solution to temper the reaction rate. Subsequently the SiO₂ layer, which can be between 2.5 and 25 nm thick, is removed from the Si substrate by dipping the sample in HF acid. The depth distribution can then be determined by measuring the intensity of the 122-keV γ peak before and after etching.

IV. EXPERIMENTAL RESULTS

After introducing the cavities and implanting the probes, the samples were annealed in order to drive a measurable amount of Co to the voids. The main question we want to address is whether trapping of the Co atoms can be established at the internal surface of the cavities. Another question then follows, namely: Under what microscopic structural environment will the trapped ⁵⁷Co/⁵⁷Fe atoms be present? Both questions can to a large extent be answered by the Mössbauer spectra.

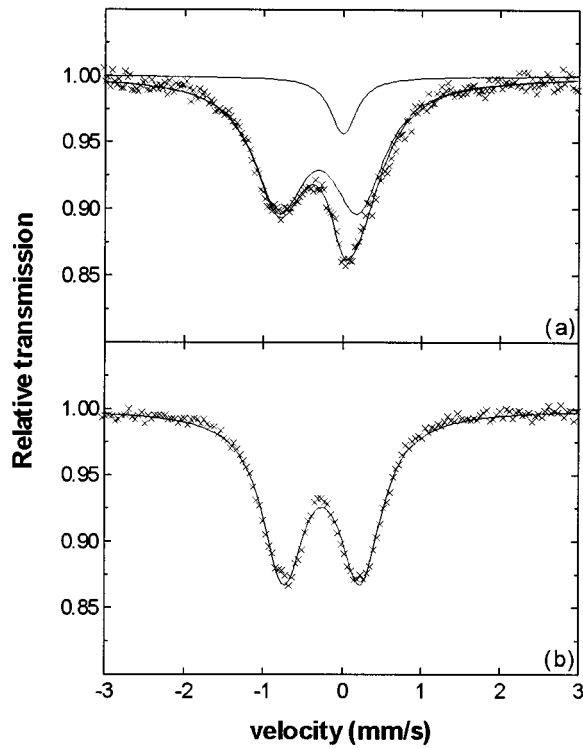


FIG. 1. Mössbauer spectra after ^{57}Co implantation at RT: (a) 80 keV implantation with a fluence of 3×10^{13} atoms/cm 2 and (b) 80 keV implantation with a fluence of 2×10^{14} atoms/cm 2 .

A. Spectra after implantation

Many systematic Mössbauer studies have been performed on ^{57}Co diffused or implanted into Si. For implantations at RT, Langouche *et al.* observed two dose-dependent contributions in the as-implanted spectra:^{20,21} a dominant quadrupole doublet and a single line. The first belongs to probes that are immobilized at the damage of their own collision cascade. The second is associated with probes on a substitutional lat-

TABLE I. Fit parameters after ^{57}Co implantation compared with the reference values from Refs. 20 and 21.

	Doublet			Single line	
	δ (mm/s)	Δ (mm/s)	W (mm/s)	δ (mm/s)	W (mm/s)
Measured	-0.32 (4)	1.0 (1)	0.8 (1)	0.00 (2)	0.4 (1)
Reference	-0.36 (3)	1.0 (1)	0.8 (1)	-0.03 (2)	0.4 (1)

tice site. The fractional occupation of the latter decreases for increasing fluences until the implanted layer becomes completely amorphous. We observed both components with the expected parameters and dose dependence, as can be seen from Fig. 1 and Table I.

B. Spectra after thermal treatment and etching

Sample *a* was vacuum annealed isothermally at 700 °C during a total time of 80 h. The surface fraction at the voids increases up to $c \approx 15\%$ with the square root of the annealing time, as can be seen from Fig. 2. For the case of Cu or Ni this fraction increases linearly until saturation occurs.³ The theoretical curve in Fig. 2 is obtained from such a simple model assuming irreversible and strong trapping from an infinite supply to an unsaturated, deep sink, with both trapping regions having a negligible thickness compared to their separation distance Δx . The steady-state diffusion flux then becomes

$$\Phi \sim \frac{n_s D}{\Delta x},$$

where n_s is the solid solubility in equilibrium and D is the diffusion coefficient.⁹ Saturation is only expected for populations of circa 5×10^{14} atoms/cm 2 ,³ far beyond the value reached after the employed annealing. It is clear that the measured values do not follow this theoretical model. This could be explained by the fact that in the initial situation the Co atoms are neither trapped at the voids nor at silicide pre-

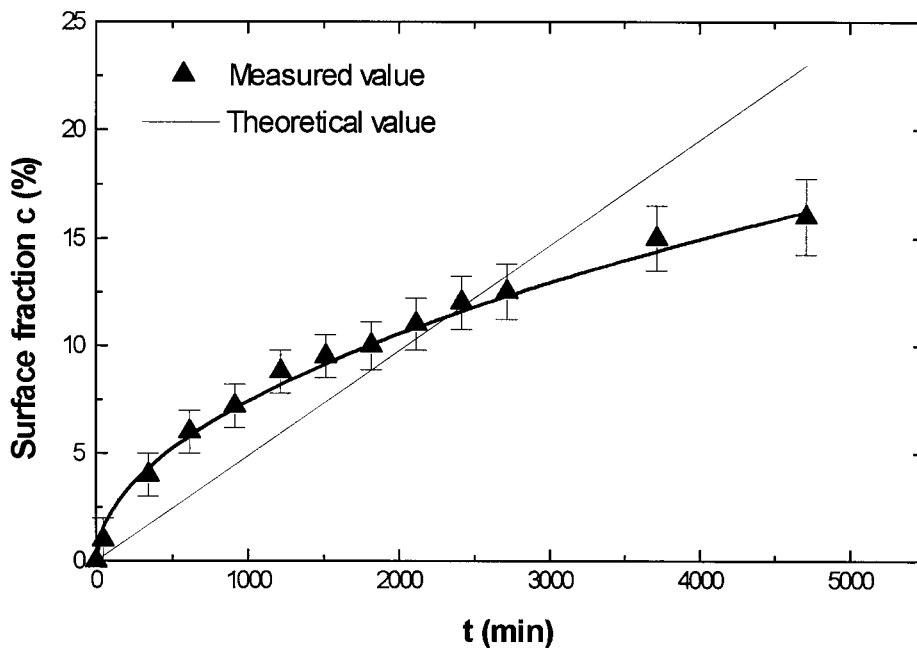


FIG. 2. Measured and theoretical value for the surface fraction c as a function of the total annealing time for sample *a*. The solid curve through the experimental data is a least-squares fit of the data as a function of \sqrt{t} .

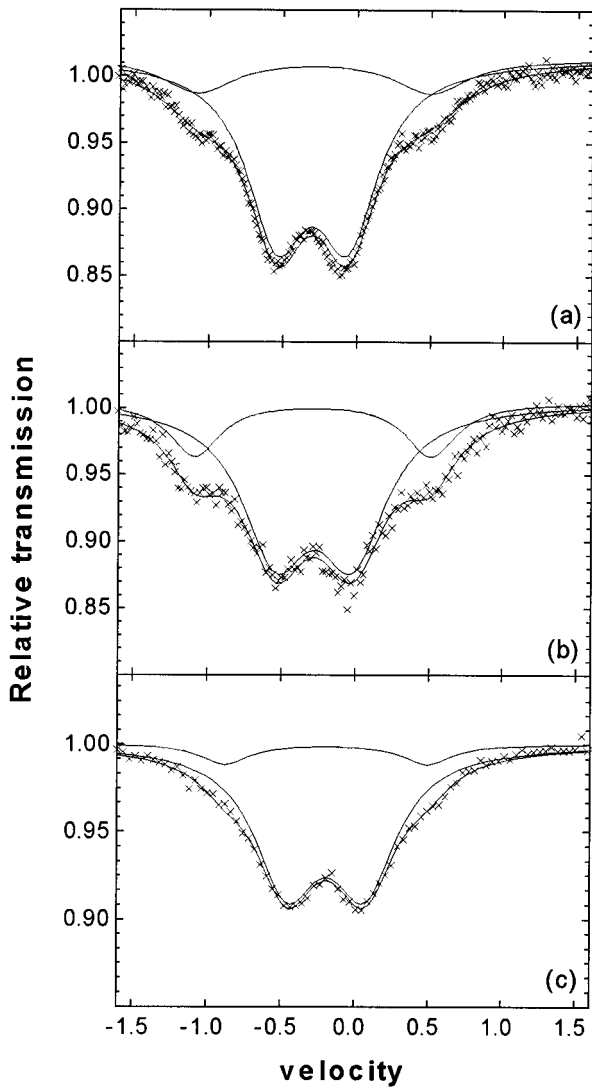


FIG. 3. Mössbauer spectra for samples *a*, *b*, and *c* after thermal treatment and etching. The solid lines represent the fitted individual components while the solid curve through the data is the resulting best fit.

precipitates, but they are situated at their own correlated implantation damage. Therefore there is not a clear redistribution from a silicide phase to the voids under steady-state conditions. Moreover, the diffusion of Co in Si is complex and not yet fully understood, so numerical calculations are subject to large uncertainties. In Sec. V we will return to this discussion. The sample was then etched on the Co-implanted side over a depth of 200 nm and on the void side over a depth of 140 nm. Only 2% of the activity diffused through the cavity

layer and is present within the topmost 10 nm as small silicide precipitates.¹⁹ At the Co-implanted side, 60% is still trapped at the correlated implantation damage while 25% is present in the topmost surface layer. The fraction at the voids then is 13% or 3×10^{13} atoms/cm². This number is in good agreement with the value stated above. Silicide formation is clearly hampered by a very efficient gettering mechanism since CoSi₂ has a large solution enthalpy and is normally formed already during diffusion.¹⁸ The Mössbauer spectrum after annealing and etching is shown in Fig. 3(a). This kind of spectrum has, to our knowledge, never been observed before and was fitted with two doublets (see Table II for fit parameters).

Sample *b* was annealed at 750 °C during 7 h. The fraction at the void side is $c \approx 32\%$. Etching yields a fraction of 45% or 4.5×10^{12} atoms/cm² at the cavities while theory yields 90%. Figure 3(b) shows the spectrum after annealing and etching. The similarity with sample *a* is apparent although Q_2 is slightly more prominent. After etching, the sample was further annealed at 750 °C during 7 h. Within the experimental error only $W(Q_1)$ changed from 0.54 (2) mm/s to 0.45 (2) mm/s.

Sample *c* was annealed at 700 °C during a total time of 30 h. It should be recalled that for this sample the activity was preimplanted at the same side and as close as possible to the cavities. The observed spectrum after annealing and etching is shown in Fig. 3(c). While all other hyperfine parameters remained unaltered with increasing annealing times, a noticeable increase of $\Delta(Q_2)$ was observed, as can be seen from Fig. 4. Approximately 60% of the Co is found residing at the cavities or 1×10^{14} atoms/cm² while theory yields 100%. Furthermore, 20% of the Co activity is trapped in small CoSi₂ precipitates in the topmost layer of the implanted side. The remaining fraction is still present at implantation depth. The fit parameters differ slightly from the previous ones as can be seen in Table II, but it is nevertheless clear that the same components are present.

Consistent fitting of the spectra measured at different source temperatures yields the characteristic Mössbauer temperature for both components: $\theta_M(Q_1) = (490 \pm 20)$ K and $\theta_M(Q_2) = (240 \pm 40)$ K. We prepared sample *d* to ascertain the formation of CoSi₂ when only implantation damage is present. We introduced the damage by Si implantation, which we then monitored as a function of thermal treatment by RBS-C measurements.¹² A clearly different behavior was observed compared to the case where voids are present, both for the Mössbauer (Fig. 5) as well as for the RBS-C measurements. The sample was annealed isochronically during 3 h starting at 500 °C up to 900 °C. After implantation, all Co atoms are situated at the damage site (see Sec. IV A). Al-

TABLE II. Fit parameters after thermal treatment and etching.

Sample	Q_1			Q_2		
	<i>a</i>	<i>b</i>	<i>c</i>	<i>a</i>	<i>b</i>	<i>c</i>
δ (mm/s)	-0.30 (2)	-0.30 (2)	-0.20 (2)	-0.28 (2)	-0.29 (2)	-0.20 (2)
Δ (mm/s)	0.48 (2)	0.51 (2)	0.50 (2)	1.59 (5)	1.64 (5)	1.42 (5)
W (mm/2)	0.49 (2)	0.54 (2)	0.53 (2)	0.37 (2)	0.47 (4)	0.42 (4)
I (%)	84 (2)	76 (4)	90 (2)	16 (2)	24 (3)	10 (2)

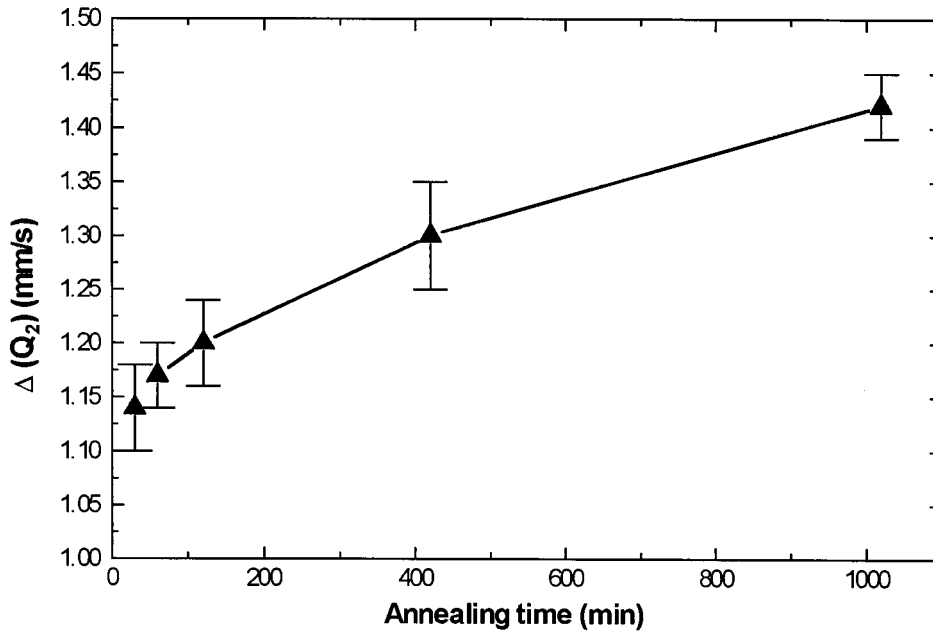


FIG. 4. $\Delta(Q_2)$ as function of annealing time at 700 °C for sample *c*.

ready after the first anneal the spectrum strongly resembles that of CoSi_2 although normally the line shape of this phase only becomes predominant after annealing at ~ 600 °C.²² This can be explained by the presence of the extra lattice damage in the Si-rich environment, resulting in fast relaxation. As higher temperatures are employed, the spectra evolve towards the spectrum for bulk CoSi_2 (Ref. 21) due to further lattice recrystallization and Ostwald ripening.

V. DISCUSSION AND INTERPRETATION

Annealing at temperatures between 600 °C and 800 °C transforms the point defects of sample *d* into extended defects,⁴ nucleating silicide formation very fast and easily because of kinetic arguments.²³ Cavities cause a lot of strain to that of extended defects, forming a competitive sink. Comparing the Mössbauer spectra of the samples with voids and the sample with secondary defects, however, proves that the trapping mechanism and sites are quite different. In case voids are present, clearly a strong and efficient gettering mechanism is active, resulting in a hampering of silicide formation during annealing. Until now silicide precipitation could only be avoided by formation of Co-acceptor pairs in highly doped *p*-type Si, but these structures break up at temperatures above 300 °C.²⁴ Nevertheless, we observe that still a considerable fraction of the Co atoms is not trapped at the voids after annealing and this is not yet fully understood. It could be that due to contamination during sample manipulation, the voids are saturated by atoms other than the Co or that the number of available sites is smaller than expected due to a local reconstruction of the surface. Another explanation, however, is that, during annealing, the amount of Co atoms in solution splits up in two fractions migrating to the two competing sinks, which are then populated by a mainly kinetic driving force²³ until there are no more Co atoms left to be trapped. The first fraction consists of the Co atoms diffusing to the rather “distant” voids while the second consists of Co atoms diffusing to small precipitates at the “nearby” surface. The latter process cannot be avoided kinetically since this sink is much closer to the initial position of the Co atoms, implying a higher diffusion flux. Indeed, we see that for sample *c* the trapped fraction at the voids is much higher than for sample *a* even when the latter has been annealed more than twice as long. This diffusion-controlled population mechanism is also supported by Fig. 2 where the fraction of the Co atoms, which is trapped at the voids, increases according to a $t^{1/2}$ behavior, typical for diffusion-controlled reaction kinetics. Once the precipitates are

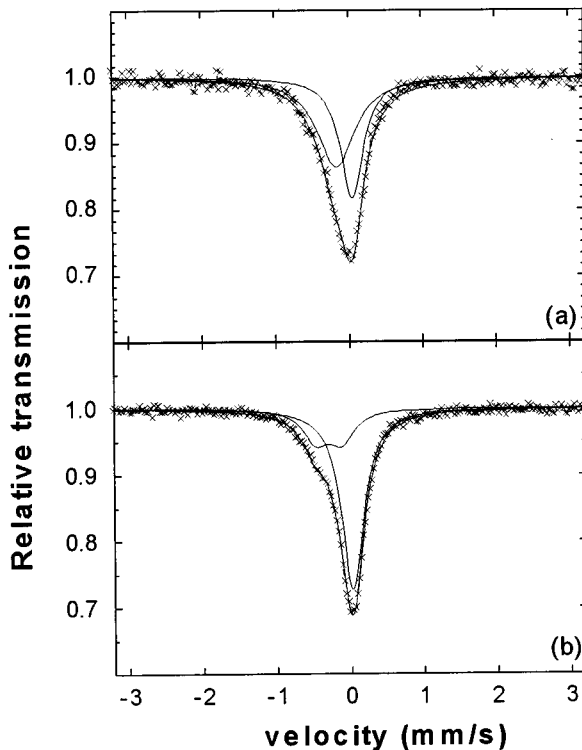


FIG. 5. Mössbauer spectra for sample *d*: after annealing at 500 °C (a) and at 900 °C (b). The solid lines represent the fitted individual components while the solid curve through the data is the resulting best fit.

formed, this fraction is difficult to be altered upon further annealing because of the high thermal stability of the silicide phase. On the other hand, the fact that the spectra do not change significantly upon long-time annealing at elevated temperatures indicates that the binding stability of the Co atoms bound to the voids is at least comparable to that of the CoSi_2 phase.

Although hardly anything is known yet about the microscopic nature of this kind of complex systems, we would like to formulate at least a preliminary interpretation. It is clear from the Mössbauer results that the voids give rise to at least two new getter sites, characterized by their hyperfine interaction parameters. Following Myers *et al.*, it is straightforward to correlate these new sites to atoms trapped at the inner wall of the cavities. Within this point of view one $^{57}\text{Co}/^{57}\text{Fe}$ atom ($3d^7 4s^2/3d^6 4s^2$) is then bound to more than one Si DB, yielding a surface coverage considerably closer to that of Ni ($3d^8 4s^2$) ($\approx 10^{14}$ atoms/cm²) than to that of Cu ($3d^{10} 4s^1$) ($\approx 5 \times 10^{15}$ atoms/cm²).³ Site 1 (Q_1) is found to be more strongly bound with $\theta_M(Q_1) \sim 490$ K, but it has the smallest electric-field gradient $V_{zz}(Q_1) = (2.3 \pm 0.2) \times 10^{17}$ V/cm². This can be explained by a site at an edge or a corner of a faceted cavity. Site 2 (Q_2) is more loosely bound with $\theta_M(Q_2) \sim 240$ K but $V_{zz} = (6.9 \pm 0.3) \times 10^{17}$ V/cm² is larger. This component is ascribed to a surface site where the atom is residing atop the Si atoms that form the faces of the cavity. The surface site has a large V_{zz} due to a more localized charge distribution in the region between the bound atom and the Si surface. At the same time, this decreases the bonding strength, leading to a smaller value for θ_M . The values of V_{zz} are in agreement with commonly observed values for probe atoms at surfaces and interfaces,^{25,26} although values for semiconductors are very scarce. Krausch *et al.* report theoretical calculations of V_{zz} for an In-probe atom residing atop a Si(111) plane and for an atom that is eclipsed within the (111) plane. The values they find are $V_{zz} = 2.1 \times 10^{18}$ V/cm² and $V_{zz} = 1.4 \times 10^{18}$ V/cm², respectively.²⁶ Although the absolute values differ substantially from our experimental observations (the values measured by Krausch *et al.* are also considerably lower than the theoretical predictions), the trend towards decreasing V_{zz} values for more eclipsed probe atoms is prominent. The increase of $\Delta(Q_2)$ with annealing time as observed for sample *c* (Fig. 4) can then be explained by the increasing degree of faceting. The similarity between $\alpha(Q_1)$ and $\delta(Q_2)$ points to a comparable binding mechanism for both sites. The linewidths $W(Q_1)$ and $W(Q_2)$ are rather small, indicating well-defined sites. Also here we can interpret the decrease of Γ as the annealing time increases as a result of the further

faceting of the cavities and hence a smaller distribution of the hyperfine interaction parameters of both sites. The observation that $W(Q_1)$ is always somewhat higher than $W(Q_2)$ can be understood by the fact that an edge site is less well determined than a surface site, since there are many different kinds of edges with different degrees of sharpness, etc., each giving rise to a slightly different set of interaction parameters. The stronger binding of the edge site explains why it is preferentially populated although it is outnumbered by the surface site by a ratio of typically 5:1. We find a number in the order of 1 populated surface site per 5 occupied edge sites. Unless the DB's are populated by atoms other than the implanted Co atoms or that some local relaxation takes place at the surface reducing the number of available DB's, this suggests that the voids are not yet fully saturated. Finally, it is worth mentioning that $I(Q_2)$ apparently depends on the local atomic concentration of the He implantation and hence on the size of the voids:⁶ the largest fraction is found for sample *b*, which also contains the largest voids and thus the largest surface-to-edge ratio. The smallest fraction is found for sample *c*, which had the smallest atomic concentration of He atoms.

VI. CONCLUSION

We experimentally found a new characteristic Mössbauer spectrum for ^{57}Co implanted in *c*-Si after nanosized voids were introduced and after thermal treatment above 700 °C. We tentatively ascribe the observed spectrum to two getter sites at the empty voids by comparison with a sample where no voids were present. The first site is more strongly bound and is preferentially populated compared to the more loosely bound site, which has the larger field gradient V_{zz} . Within the model we present, this difference is due to a more localized binding geometry of the latter. This nanosystem offers both very intriguing physical as well as application-oriented perspectives. In the future we hope to obtain higher coverages and controllability and to determine a value of the solution enthalpy of both sites by following the dynamics of the gettering more closely, especially the competition between silicide formation and trapping at the voids. Comparison with Mössbauer spectra of ^{57}Co atoms that are to be deposited by soft landing on clean external surfaces form an excellent basis for a variety of further "clean-surface" experiments.

ACKNOWLEDGMENTS

W.D. is grateful to the NFWO (National Fund for Scientific Research, Belgium) for financial support.

*Electronic address: wim.deweerd@fys.kuleuven.ac.be

†Also with Soreq Nuclear Research Center, Yavne, Israel.

¹Klaus Graff, *Metal Impurities in Silicon-Device Fabrication* (Springer-Verlag, Berlin, 1995).

²D. Gilles, in *Defect Engineering in Semiconductor Growth, Processing and Device Technology*, edited by S. Ashok, J. Chevalier, K. Sumino, and E. Weber, MRS Symposia Proceedings No. 262 (Materials Research Society, Pittsburgh, 1992), p. 917.

³S. M. Myers, D. M. Folstaedt, and D. M. Bishop, in *Materials Synthesis and Processing Using Ion Beams*, edited by R. J. Cul-

bertson, O. W. Holland, K. S. Jones, and K. Maex, MRS Symposia Proceedings No. 316 (Materials Research Society, Pittsburgh, 1994), p. 33.

⁴J. Wong-Leung, J. S. Williams, R. G. Elliman, E. Nygren, D. J. Eaglesham, D. C. Jacobson, and J. M. Poate, Nucl. Instrum. Methods Phys. Res. Sect. B **96**, 253 (1995).

⁵M. H. F. Overwijk, J. Politiek, R. C. M. de Kruif, and P. C. Zalm, Nucl. Instrum. Methods Phys. Res. Sect. B **96**, 257 (1995).

⁶V. Raineri, A. Battaglia, and E. Rimini, Nucl. Instrum. Methods Phys. Res. Sect. B **96**, 249 (1995).

- ⁷S. P. Murarka, *Silicides for VLSI Applications* (Academic, New York, 1983).
- ⁸J. M. Gibson, R. T. Tung, and J. M. Poate, in *Defects in Semiconductors II*, edited by S. Mahajan and J. W. Corbett, MRS Symposia Proceedings No. 14 (Materials Research Society, Pittsburgh, 1983), p. 395.
- ⁹E. R. Weber, *Appl. Phys.* **A30**, 1 (1983).
- ¹⁰C. C. Griffioen, J. H. Evans, P. C. De Jong, and A. Van Veen, *Nucl. Instrum. Methods Phys. Res. Sect. B* **27**, 417 (1987).
- ¹¹D. M. Follstaedt, *Appl. Phys. Lett.* **62**, 1116 (1993).
- ¹²W. Deweerdt, R. Moons, G. Langouche, H. Pattyn, and J. Verheyden (unpublished).
- ¹³B. Mohadjeri, J. S. Williams, and J. Wong-Leung, *Appl. Phys. Lett.* **66**, 1889 (1995).
- ¹⁴S. T. Picraux, in *Defects in Semiconductors*, edited by Narayan and Tan (North-Holland, Amsterdam, 1981), p. 135.
- ¹⁵W. Bergholz, *Phys. Status Solidi A* **49**, 489 (1978).
- ¹⁶*Semiconductors, Hyperfine Interaction of Defects in Semiconductors*, edited by G. Langouche (Elsevier, Amsterdam, 1992).
- ¹⁷D. G. Rancourt, *Nucl. Instrum. Methods Phys. Res. Sect. B* **44**, 199 (1989).
- ¹⁸J. Utzig, *J. Appl. Phys.* **67**, 3629 (1988).
- ¹⁹W. Bergholtz, *J. Phys. D* **14**, 1099 (1981).
- ²⁰G. Langouche and M. De Potter, *Nucl. Instrum. Methods Phys. Res. Sect. B* **19/20**, 322 (1987).
- ²¹G. Langouche, M. De Potter, I. Dézsi, M F. Wu, and A. Vantomme, *Nucl. Instrum. Methods Phys. Res. Sect. B* **37/38**, 438 (1989).
- ²²I. Dézsi, H. Engelman, U. Gonser, and Guido Langouche, *Hyperfine Interact.* **33**, 161 (1987).
- ²³M. Seibt and W. Schröter, *Solid State Phenom.* **19&20**, 283 (1991).
- ²⁴A.-M. Van Bavel, Ph.D. thesis, K. U. Leuven, 1995, p. 31.
- ²⁵H. Pattyn, P. Hendrickx, and S. Bukshpan, *Proceedings of Nato A.R.W. in Fundamental Aspects of Inert Gases in Solids*, edited by S. E. Donnelly and J. H. Evans (Plenum, New York, 1991), p. 243.
- ²⁶G. Krausch, T. Detzel, R. Fink, B. Luckscheiter, R. Platzer, U. Wöhrmann and G. Schatz, *Phys. Rev. Lett.* **68**, 377 (1992).